frontiers | Frontiers in Physics

TYPE Original Research
PUBLISHED 18 April 2023
DOI 10.3389/fphy.2023.1159306

OPEN ACCESS

EDITED BY
Nirpendra Singh,
Khalifa University, United Arab Emirates

REVIEWED BY
Manish Pratap Singh,
Veer Bahadur Singh Purvanchal University, India
Deepika Jamwal,
Panjab University, India

*CORRESPONDENCE
Noureddine Mahdhi,
noureddine.maadhi@fst.rnu.tn
Saber Hammami,
saber.hammami@crhea.cnrs.fr

SPECIALTY SECTION
This article was submitted to Interdisciplinary Physics, a section of the journal Frontiers in Physics

RECEIVED 05 February 2023
ACCEPTED 20 March 2023
PUBLISHED 18 April 2023

CITATION
Mahdhi N, Alsaiari NS, Amari A, Osman H and Hammami S (2023), Enhancement of the physical adsorption of some insoluble lead compounds from drinking water onto polylactic acid and graphene oxide using molybdenum disulfide nanoparticles: Theoretical investigation. *Front. Phys.* 11:1159306. doi: 10.3389/fphy.2023.1159306

Enhancement of the physical adsorption of some insoluble lead compounds from drinking water onto polylactic acid and graphene oxide using molybdenum disulfide nanoparticles: Theoretical investigation

Noureddine Mahdhi[1]*, Norah Salem Alsaiari[2], Abdelfattah Amari[3], Haitham Osman[3] and Saber Hammami[4]*

[1]Laboratory Materials Organizations and Properties, Department of Physics, Faculty of Science of Tunis, University of Tunis El Manar, Tunis, Tunisia, [2]Department of Chemistry, College of Science, Princess Nourah bint Abdulrahman University, Riyadh, Saudi Arabia, [3]Department of Chemical Engineering, College of Engineering, King Khalid University, Abha, Saudi Arabia, [4]Centre de Recherche pour l'Hétéro-Epitaxie et ses Applications, Centre National de La Recherche Scientifique, Université Côte d'Azur, Valbonne, France

This study reports the enhancement of the physical adsorption of some insoluble lead compounds, from drinking water, onto polylactic acid (PLA) polymer and graphene oxide (GO) by filling with molybdenum disulfide (MoS_2) nanoparticles (NPs). Based on the Lifshitz theory, we demonstrate the attractive nature of the van der Waals (vdW) interactions that are responsible for the physical adsorption between the cerussite ($PbCO_3$), the pyromorphite ($Pb_5(PO_4)_3Cl$), and the lead dioxide (PbO_2) insoluble adsorbates and the GO/MoS_2 and PLA/MoS_2 adsorbent nanocomposites in water medium. Subsequently, we show an increase in the physical adsorption, at close and large separation distances (<100 nm) in the water medium, between the lead-insoluble adsorbate and the adsorbent GO/MoS_2 and PLA/MoS_2 nanocomposites by increasing the filling ratios (0%, 10%, 20%, and 30%) of MoS_2 NPs. Moreover, for each lead-insoluble adsorbate, we demonstrate that the vdW adsorption potential and force were more important for GO/MoS_2 than for PLA/MoS_2 adsorbent. However, for a fixed filling rate, the physical adsorption was more important in the order PbO_2 > $Pb_5(PO_4)_3Cl$ > $PbCO_3$. Interestingly, we demonstrate that the physical adsorption strongly depended on the GO/MoS_2 and PLA/MoS_2 adsorbent type and weakly dependent to the lead compound adsorbates. For all "PbO_2, $Pb_5(PO_4)_3Cl$, and $PbCO_3$" adsorbates, we demonstrate that the vdW adsorption potential and force were higher ~6, ~3.1, ~2.2, and ~1.9 times for GO than for PLA adsorbent for, respectively, filling ratios 0%, 10%, 20%, and 30% of MoS_2 NPs.

KEYWORDS

physical adsorption, polylactic acid, graphene oxide, molybdenum disulfide, lead compounds, insoluble, drinking water

1 Introduction

Despite the implementation of filtration and purification processes for drinking water, some lead-insoluble compounds remain persisting in domestic drinking water [1–3]. Recently, cerussite ($PbCO_3$), pyromorphite ($Pb_5(PO_4)_3Cl$), and lead dioxide (PbO_2) are among the most hazardous insoluble lead compounds that persist in drinking water distribution systems [2–4]. They are leached in drinking water primarily from corrosive water effects on the household plumbing systems containing lead in pipes, solder, or fittings or from the service connections to homes, galvanic corrosion [4–6]. According to the World Human Organization (WHO), the presence of lead and lead compounds in drinking water causes many hazardous human health diseases, such as neurotoxicity, mutagenicity, and carcinogenicity [7].

There are many physic-chemical purification processes for drinking water, such as photocatalysis, chemical adsorption, reverse osmosis, and chemical coagulation [8, 9]. However, these processes include some disadvantages, essentially high cost-effectiveness and energy consumption [10, 11], lack of solar sensitivity and lower efficiency [11], precipitation of insoluble substances during coagulation-flocculation [12], and removal of the essential multivalent and all monovalent minerals ions required for the human body [13]. In addition to their insolubility in the water medium, the PbO_2, $PbCO_3$, and $Pb_5(PO_4)_3Cl$ compounds require higher decomposition temperatures of 588 K, 613 K, and 1,373 K, respectively [14, 15], which makes it very difficult to remove these compounds from drinking water by the previous processes. Moreover, these processes generally comprise the chemical procedure, which may allow the release of a secondary product and the rise in temperature and consequently affect the drinking water quality.

Adequately, physical adsorption is a suitable purification process for this case study. In fact, physical adsorption allows the removal of solid contaminants from water at room temperature and pressure and can operate simultaneously with other purification processes [16, 17]. In contrast to the previously cited process, physical adsorption is low-cost, simple, and easy to design, and no activation energy is necessary. It possesses high running speed compared to other purification processes, is of reversible nature, occurs on many solid surfaces, can remove multimolecular layers, and is performed under normal temperature and pressure conditions [16–18]. In addition, the physical adsorption process can be implemented essentially in a gravity microfilter, which allows the purification of the drinking water without any additional energy.

Nowadays, graphene oxide (GO), polylactic acid (PLA), and molybdenum disulfide (MoS_2) have received much attention in the research area of the water purification community. The purification efficiency of drinking water has been largely investigated by photocatalysis and membrane separation [19–21]. In fact, GO, PLA, and MoS_2 are promising materials for the application in the physical adsorption process because their natural abundantly, biocompatibility, wide variety of preparation procedures with different size and shape particles [22–24].

Currently, no previous research has investigated the examination of the physical adsorption of the insoluble lead compounds, "$PbCO_3$, $Pb_5(PO_4)_3Cl$, and PbO_2," onto PLA and GO filled with MoS_2 NPs in the water medium.

In this work, we examine the physical adsorption of the lead compounds "$PbCO_3$, $Pb_5(PO_4)_3Cl$, PbO_2" onto GO, PLA matrixes filled with MoS_2 NPs in the water medium. First, using the Lifshitz theory, we evaluate the strength and type of van der Waals (vdW) interactions responsible for the physical adsorption by the calculation of the Hamaker constant at large and close separation distance between lead adsorbate and (GO/MoS_2, PLA/MoS_2) nanocomposites in water medium. Afterward, the investigation of the vdW adsorption potential and force as a function of the filling rates of the MoS_2 NPs of the GO and PLA matrix and the lead adsorbate type were made. Later, an enhancement of the adsorption by increasing the refractive index of the adsorbate and adsorbent in a water medium will be demonstrated. Eventually, a comparative study demonstrates that physical adsorption is highly sensitive to the adsorbent type and poorly depends on the adsorbate type.

2 Materials and methods

2.1 Materials

Adsorbent materials investigated in this study are the PLA polymer and GO filled with MoS_2 NPs. The thickness of the adsorbent nanocomposites is considered to be above 1 μm to ensure that the nanoparticle fillers, with an average size of a few nanometers (~5 nm), were uniformly dispersed in the PLA and GO matrixes. The volume fraction Φ = (0%, 10%, 20%, and 30%) is defined as the percent volume fraction of the MoS_2 NPs of the total volume of the nanocomposite mixture. The adsorbates examined in this study are the water-insoluble lead compounds $PbCO_3$, PbO_2, and $Pb_5(PO_4)_3Cl$.

Hereafter, the proposed rates of volume fraction of MoS_2 NPs added to PLA and GO matrixes are designated and summarized in Table 1.

2.2 Methods

2.2.1 vdW adsorption potential and force

In this work, physical adsorption designs the adhesion of the lead compound particles onto a nanocomposite surface in a water medium under the action of intermolecular surface forces. Essentially, physical adsorption is driven by hydrogen binding, hydrophobic interactions, and vdW intermolecular forces, which include Keesom, Debye, and London forces [16–18, 25].

TABLE 1 Designation of GO/MoS_2 and PLA/MoS_2 nanocomposites as a function of volume fraction of MoS_2 filler rates.

Φ (%) of MoS_2 NPs	Nanocomposite	
	GO/MoS_2	PLA/MoS_2
0	GO	PLA
10	$GO/10MoS_2$	$PLA/10MoS_2$
20	$GO/20MoS_2$	$PLA/20MoS_2$
30	$GO/30MoS_2$	$PLA/30MoS_2$

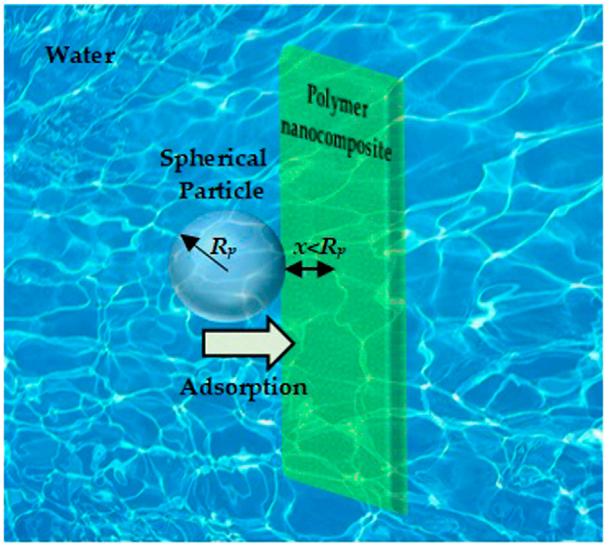

FIGURE 1
Schematic illustration of the physical adsorption: spherical particle adsorbate with radius R_p located near flat adsorbent nanocomposite surface in a water medium at separation distance ($x << R_p$).

However, in the aqueous medium, the water molecules are expected to occupy a large portion of the H-bonding sites [26]. Consequently, the hydrogen binding is reasonably ignored because the adsorbent and adsorbate were fully hydrated by extending their contact with water [27]. Additionally, for water-insoluble compounds, the hydrophobic interactions are much larger. Then, the higher the affinity, the greater the extent of the adsorption with other near materials [28]. Consequently, the insolubility of such lead compounds constitutes a favor factor for their physical adsorption onto PLA/MoS_2 and PLA/MoS_2 nanocomposite adsorbent from water medium.

Therefore, the physical adsorption of the insoluble lead compound onto the surface of PLA/MoS_2 and PLA/MoS_2 nanocomposites is driven solely by the vdW forces in a water medium. Hence, the physical adsorption was called vdW adsorption. Subsequently, the essential purpose of this study is to evaluate the type and strength of the vdW interaction potential and force between the insoluble lead compound and the GO/MoS_2 and PLA/MoS_2 nanocomposite adsorbate in the water medium.

As shown in Figure 1, the lead compound particle is assimilated to a spherical particle of a radius R_p (adsorbate) that reign in a water medium near a flat surface of the composites (adsorbent) at the distance $x << R_p$.

For the evaluation of the vdW interactions, we used the computational methods that have demonstrated good accordance between theoretical and experimental results by many recent studies for evaluating the intermolecular vdW interactions either for accounting for the adhesion force and energy and the adsorption of a variety of materials liquids in aqueous media [25, 29–31].

According to Figure 1, the fully vdW potential involving the adsorption along the separation distance ($x \leq 100$ nm) is given as follows [31]:

$$U_{vdW}(x) = -\left[A_{v=0}^{ret} + A_{v>0}^{ret}\right]\frac{R_p}{6x} = -\left[A_{v=0}e^{-\kappa x} + \frac{A_{v>0}}{1+14x/100}\right]\frac{R_p}{6x}, \quad (1)$$

where $A_{v=0}^{ret}$ and $A_{v>0}^{ret}$ are, respectively, the retarded polar and dispersive parts of the Hamaker constants. $A_{v=0}$ is the zero-frequency, also called non-retarded Hamaker constant, which regroups the Keesom interactions arising from permanent molecular dipoles and Debye interactions arising from permanent and induced dipoles' polar vdW interactions [32, 33]. For drinking water, the non-retarded Keesom and Debye interactions are reduced proportionally by $e^{-\kappa x}$ along the interacting distance $x \leq 100$ nm under the action of the conduction effects [31, 34], where κ^{-1}, known as the Debye screening length, equals 960 nm for drinking water with pH 7 [31].

In contrast, $A_{v>0}$ is the non-zero-frequency, also called non-retarded, Hamaker constant, including the London dispersion interactions that result from the fluctuations in the charge densities of the electron clouds surrounding the nuclei of the atoms [35]. Along the separation distance ($x \leq 100$ nm), Gregory stated that $A_{v>0}$ became retarded ($A_{v>0}^{ret}$) and it reduced approximately by 1/(1 + 14x/100) [36].

2.2.2 vdW adhesion energy and force

Once the spherical lead particle is submitted to the attractive vdW interactions from the nanocomposite surface in a water medium, it will be adsorbed onto the nanocomposite surface under the action of the vdW adhesion energy expressed analytically by [31]:

$$U_{adh} = -(A_{v=0} + A_{v>0})\frac{R_P}{6.x_0}, \quad (2)$$

where x_0 is the closet separation distance between adsorbent and adsorbate molecules after adsorption. It is called the cut-off distance and typically equals 0.165 nm.

The correspondent adhesion force involved by the vdW interactions responsible for the physical adsorption is expressed as [31]:

$$F_{adh} = -(A_{v=0} + A_{v>0})\frac{R_P}{6.x_0^2}. \quad (3)$$

2.2.3 Hamaker constant

The Hamaker constant was calculated using the Lifshitz theory, allowing for easy and rigorous analytical calculation of vdW interactions between any two macroscopic media 1 and 2 interacting across medium 3. In such a theory, the influence of neighboring atoms on the interaction between any pair of atoms is ignored, and the materials are treated as continuous media with the same absorption frequencies [31].

The polar Hamaker constant is expressed as a function of the static dielectric constant dominated by the Keesom and Debye interactions of the interacting media:

$$A_{v=0} = \frac{3}{4}k_B T\frac{\varepsilon_1-\varepsilon_3}{\varepsilon_1+\varepsilon_3}.\frac{\varepsilon_2-\varepsilon_3}{\varepsilon_2+\varepsilon_3}, \quad (4)$$

where k_B is the Boltzmann constant, T is the temperature, ε_1, ε_2, and ε_3 are, respectively, the dielectric permittivity of the adsorbent, adsorbate, and water medium.

TABLE 2 Dielectric constants and refractive indexes of adsorbent (PLA, GO, and MoS_2) and lead-insoluble adsorbate "$PbCO_3$, $Pb_5(PO_4)_3Cl$, PbO_2" and water at room temperature (298 K).

Materials		ε at 1 MHz	*n* at 600 nm
Adsorbent materials	Polylactic acid: PLA	2.70 [37]	1.46 [38]
	Graphene oxide: GO	40 [39]	2.35 [40]
	Molybdenum disulfide: MoS_2	21.36 [41]	4.60 [42]
Adsorbate	Cerussite: $PbCO_3$	18.60 [43]	1.80 [14]
Lead compounds	Pyromorphite: $Pb_5(PO_4)_3Cl$	5.87 [44]	2.05 [14]
	Lead dioxide: PbO_2	12.50 [45]	2.30 [46]
Medium	Water	78.40 [47]	1.33 [47]

In contrast, the dispersive part of the Hamaker constant is expressed as a function of the refractive index of the three interacting media as follows [25]:

$$\mathbf{A}_{\nu>0} = \frac{3h\nu_e}{8\sqrt{2}} \frac{(n_1^2 - n_3^2)(n_2^2 - n_3^2)}{(n_1^2 + n_3^2)^{1/2}(n_2^2 + n_3^2)^{1/2}\left[(n_1^2 + n_3^2)^{1/2} + (n_2^2 + n_3^2)^{1/2}\right]}, \quad (5)$$

where ν_e is the main electronic absorption frequency in the UV, typically around 3×10^{15} s^{-1} [25], h is the Planck constant, and n_1, n_2, and n_3 are, respectively, the refractive index of the adsorbent, adsorbate, and water.

In fact, the refractive index is the root square of the dielectric constant at optical frequencies (ϵ_{opt}) as $n = \sqrt{\epsilon_{opt}}$ dominated by the London dispersion interactions.

In Table 2, the dielectric constant and the refractive index for the calculation of the Hamaker constants are obtained from the bibliography.

2.2.4 Calculation of the dielectric constant and refractive index of nanocomposites

The dielectric constant of the nanocomposite materials is calculated using the Looyenga formula by considering that the nanoparticle filler has a spherical form and is uniformly dispersed in the continuous polymer matrix [48]:

$$\boldsymbol{\varepsilon}^{1/3} = \boldsymbol{\Phi}\boldsymbol{\varepsilon}_{\mathbf{m}}^{1/3} + (\mathbf{1} - \boldsymbol{\Phi})\,\boldsymbol{\varepsilon}_{\mathbf{f}}^{1/3}, \quad (6)$$

where Φ is the volume fraction (%) of the filler and ε, ε_m, and ε_f are the dielectric constant of the nanocomposites, polymer matrix, and filler, respectively.

The refractive index of the nanocomposites is calculated using the mixing theory of Maxwell Garnet as follows [49]:

$$n^2 = n_m^2 \frac{\left(n_f^2 + 2n_m^2\right) + 2\Phi\left(n_f^2 - n_m^2\right)}{\left(n_f^2 + 2n_m^2\right) - \Phi\left(n_f^2 - n_m^2\right)}, \quad (7)$$

where n, n_m, and n_f are the refractive indexes of the nanocomposite, polymer matrix, and filler, respectively.

3 Results

All the theoretical calculations and discussions of the results were performed under normal conditions of temperature (298 K) and pressure (100 kPa). Hypothetically, the refractive index and the dielectric constant, which are intensive physical properties, are independent of the materials' size and shape and are considered isotropic for all media.

TABLE 3 Refractive index "*n*" and dielectric constant "*ε*" of nanocomposites GO/MoS_2 and PLA/MoS_2 as a function of the volume fraction (*Φ*) of MoS_2 NPs.

Φ (%) of MoS_2	GO/MoS_2		PLA/MoS_2	
	n	ε	*n*	ε
0	2.35	40	1.46	2.70
10	2.52	37.78	1.63	3.58
20	2.70	35.64	1.83	4.64
30	2.89	33.58	1.99	5.90

3.1 Evaluation of the vdW interactions between the lead compounds and nanocomposites in water medium at close and large separation

To obtain the non-retarded Hamaker on the basis of the Lifshitz theory, we first calculated the dielectric constant (Eq. 6) and the refractive index (Eq. 7) of the GO and PLA matrices at volume fraction Φ = (0%, 10%, 20%, and 30%) of the MoS_2 NPs filler. As summarized in Table 2, the n of the GO/MoS_2 and PLA/MoS_2 increases notably with the volume fraction of the MoS_2 NPs filler. As it can interpret from equation 7, this is explained by the elevated value of the refractive index of MoS_2 NPs compared to GO and PLA matrices.

However, the ε decreases for GO/MoS_2 and increases for PLA/MoS_2 nanocomposites during filling with MoS_2 NPs. This fact is explained by the higher ε of the GO and the lower ε of PLA compared to that for MoS_2 NPs.

Therefore, referring to Tables 2, 3, the non-retarded Hamaker constants $A_{\nu=0}$ and $A_{\nu>0}$ are calculated using Eqs 4, 5. In Table 4, we compiled the Hamaker constant between the adsorbent

TABLE 4 Non-retarded Hamaker constants for the interactions between adsorbent nanocomposites (GO/MoS_2 and PLA/MoS_2) and the lead-insoluble adsorbates ($PbCO_3$, $Pb_5(PO_4)_3Cl$, and PbO_2) in a water medium at 298 K.

Lead Compounds	Φ (%)	GO/MoS_2			PLA/MoS_2		
		$A_{v=0}$ (10^{-20}J)	$A_{v>0}$ (10^{-20}J)	A (10^{-20}J)	$A_{v=0}$ (10^{-20}J)	$A_{v>0}$ (10^{-20}J)	A (10^{-20}J)
$PbCO_3$	0	0.0617	9.752	9.814	0.177	1.510	1.687
	10	0.0665	10.95	11.02	0.173	3.368	3.541
	20	0.0713	12.11	12.18	0.168	5.377	5.545
	30	0.0761	13.22	13.23	0.163	6.848	7.011
$Pb_5(PO_4)_3Cl$	0	0.0861	14.18	14.27	0.247	2.182	2.429
	10	0.0929	15.94	16.03	0.242	4.872	5.114
	20	0.0996	17.65	17.75	0.235	7.791	8.026
	30	0.1063	19.31	19.42	0.228	9.935	10.16
PbO_2	0	0.0725	18.12	18.19	0.208	2.770	2.978
	10	0.0782	20.39	20.47	0.204	6.194	6.398
	20	0.0839	22.61	22.69	0.198	9.918	10.13
	30	0.0895	24.76	24.85	0.192	12.66	12.85

nanocomposites (GO/MoS_2 and PLA/MoS_2) and the lead-insoluble adsorbates "$PbCO_3$, $Pb_5(PO_4)_3Cl$, and PbO_2" in the water medium.

As shown in Table 4, all the non-retarded Hamaker constants are in good accordance with the order of magnitude of the Hamaker constant, which ranges about $\times 10^{-20}$ J [31]. Effectively, this demonstrates the preciseness of our used theoretical methods for the estimation of the vdW intermolecular interactions. Remarkably, the positive values of the non-retarded Hamaker constant demonstrate the attractive nature of the vdW intermolecular interaction between the nanocomposite adsorbents "GO/MoS_2 and PLA/MoS_2" and the "$PbCO_3$, $Pb_5(PO_4)_3Cl$, and PbO_2" adsorbates in the water medium. Interestingly, this demonstrates that the physical adsorption of the insoluble lead compounds onto the nanocomposite surface in the water medium is driven by the non-retarded vdW interactions. The findings are consistent with recent findings by Sato et al. [25] and Aoyama et al. [29], demonstrating that the vdW interactions are sufficiently strong to drive the adsorption of colloidal particle adsorption onto polymer gels in the water medium without any other special interaction.

Moreover, the non-retarded Hamaker constant (A) was dominated over >90% by the $A_{v>0}$ dispersive part. This suggests that the vdW adsorption forces were driven by the London dispersion interactions. Moreover, the strength of the A for the GO/MoS_2 was about ~2 to ~6 orders of magnitude higher than that of A for PLA/MoS_2 for all filler ratios and lead compounds. This is attributed to the high refractive index (i.e., London dispersion interactions) of GO/MoS_2 compared to those of PLA/MoS_2 nanocomposite.

Now let us discuss the evolution of the corresponding retarded Hamaker constant at a large separation distance ($x \leq 100$ nm). For depicting the contribution of the London dispersion forces and the polar Keesom–Debye on the retarded Hamaker constant, we have drawn $A^{ret}_{v=0}$ and $A^{ret}_{v>0}$ along separation distance $x \leq 100$ nm. As deduced from Figure 2, $A^{ret}_{v>0}$ (blue line) is reduced with increasing separation due to retardation effects, but it did not reach zero for all nanocomposites and lead compounds. Despite the poor contribution of the total Hamaker constant, the polar $A^{ret}_{v=0}$ vdW intermolecular interactions did not suffer retardation effects and remained constant at all separation distances and interacting systems.

Subsequently, Figure 2 shows an increase in the vdW interactions, for all adsorbents and adsorbates in the water medium, by increasing the filling with MoS_2 NPs. This fact was more important for the interactions between PLA/MoS_2 adsorbent, and it can be identified by the dispersion, as the separation becomes closer, of the curves of PLA/MoS_2 adsorbent for Φ = (0%, 10%, 20%, and 30%) (Figures 2B–F). From these results, it is important to depict the enhancement of the vdW interactions for PLA and GO adsorbent by increasing the filling rate of MoS_2 NPs.

Particularly, at large separation distances (40–100 nm), the dispersive $A^{ret}_{v>0}$ of pure PLA (Figures 2B–F) decay until overlapping the polar $A^{ret}_{v=0}$ of PLA/MoS_2 for Φ = (0%, 10%, 20%, and 30%). This particular result demonstrates that the Keesom–Debye vdW interactions, which do not suffer from retardation, remain approximately constant and become the dominant interactions compared to the London dispersion interactions at a sufficiently large separation distance.

3.2 Adsorption of lead compounds onto GO/MoS_2 and PLA/MoS_2 in water medium

Hereafter, the adsorption potential, adhesion energy, and force of lead particles onto GO/MoS_2 and PLA/MoS_2 adsorbent surfaces in the water medium are reported from the Hamaker constant. As presented in Figure 1, we consider the lead particles, with spherical shape with radius R_p = 200 nm, located near the flat adsorbent nanocomposite surface at separation distance (x = 100 nm) << R_p.

10.3389/fphy.2023.1159306

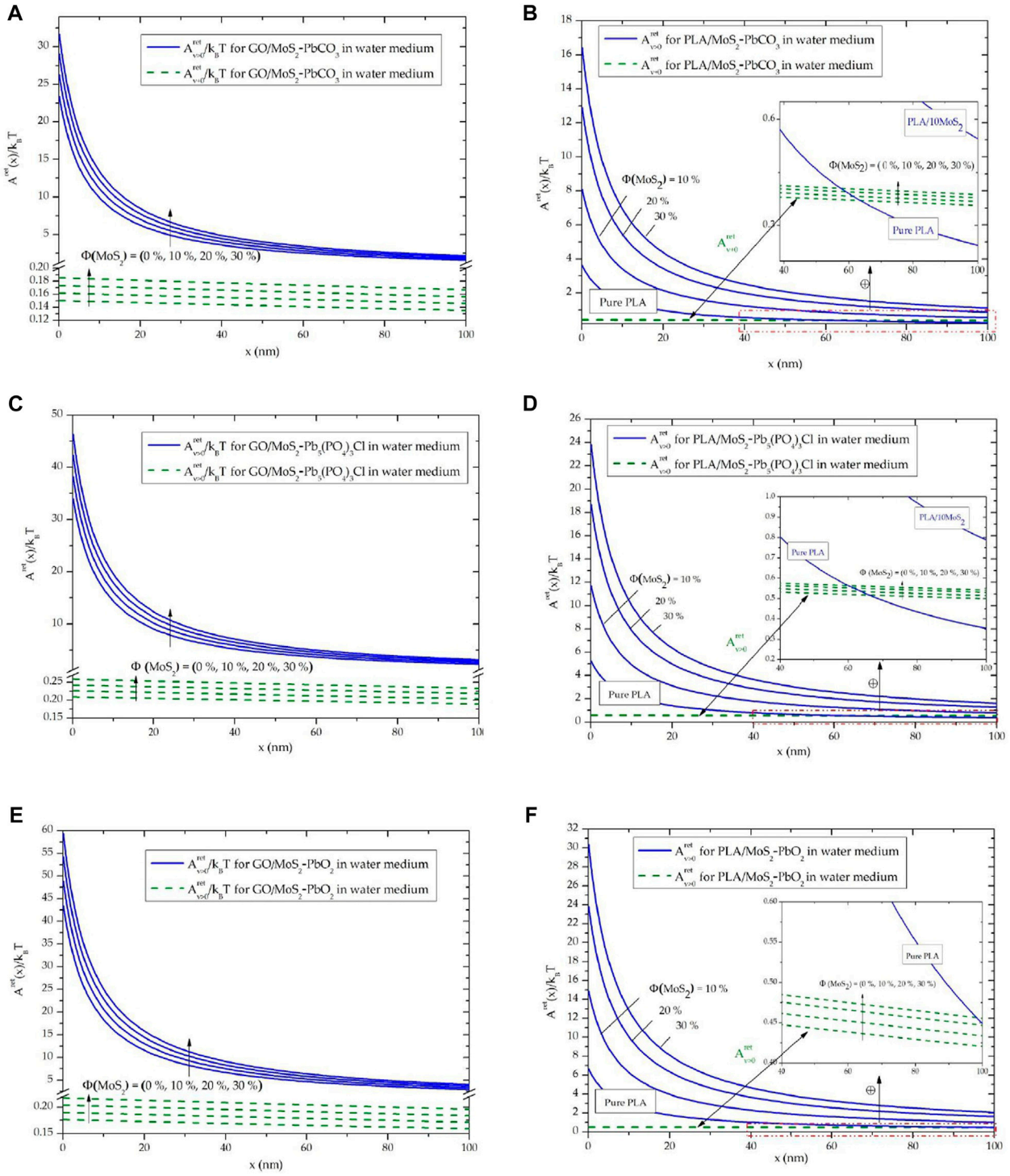

FIGURE 2
Evolution of the retarded Hamaker constant in a water medium between adsorbents and adsorbates: **(A)** GO/MoS_2-$PbCO_3$, **(B)** PLA/MoS_2-$PbCO_3$, **(C)** GO/MoS_2-$Pb_5(PO_4)_3Cl$, **(D)** PLA/MoS_2-$Pb_5(PO_4)_3Cl$, **(E)** GO/MoS_2-PbO_2, and **(F)** PLA/MoS_2-PbO_2.

3.2.1 Effect of the filling rates of the MoS_2 NPs

The evolution of the vdW potential was calculated from the retarded Hamaker constant using Eq. 1. Figure 3 depicts the evolution of $U_{vdW}(x)$ normalized to k_BT energy at Φ = (0%, 10%, 20%, and 30%) of MoS_2 NPs filler for the $PbCO_3$ adsorbate and the GO/MoS_2 and PLA/MoS_2 nanocomposite adsorbent in the water medium. For all adsorbents and $PbCO_3$ adsorbate, the vdW adsorption potential $U_{vdW}(x)/k_BT$ is a typical attractive potential

10.3389/fphy.2023.1159306

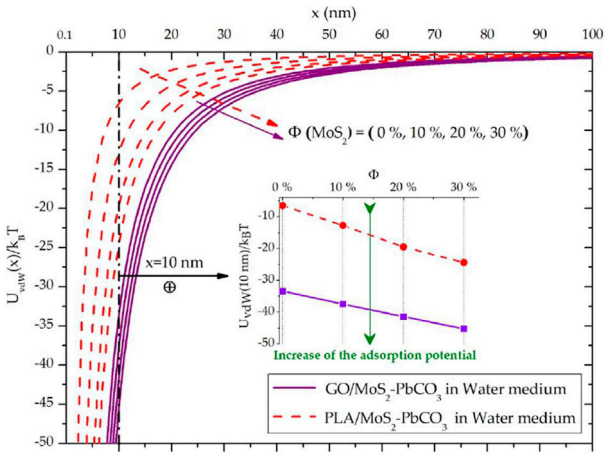

FIGURE 3
Effect of the filling rates with MoS_2 NPs on the evolution of the vdW adsorption potential between Cerussite "$PbCO_3$" adsorbate and GO/MoS_2 and PLA/MoS_2 nanocomposite adsorbents in water medium.

(negative interaction energy), which increases progressively as the separation distance becomes short [31].

For both GO/MoS_2 and PLA/MoS_2 nanocomposites, an enhancement of the vdW potential (translating from left to right in Figure 3) with increasing the filling ratios of the MoS_2 NPs is remarked. Homogeneously, this result is attributed to the greater refractive index of the MoS_2 NPs (n = 4.6) compared with the refractive index of the GO (n = 2.35) and PLA (n = 1.46) (Table 1), which consequently involves an increase in the vdW dispersion forces that drive over 90% of the vdW interactions. As mentioned in Figure 3, for x = 10 nm, we demonstrate the enhancement of the adsorption potential U_{vdW} (10 nm)/k_BT with Φ = (0%, 10%, 20%, and 30%), which increases from ~33.k_BT to ~45.k_BT, respectively, for GO and GO/30MoS_2, and from ~6.k_BT to ~24.k_BT, respectively, for PLA and PLA/30MoS_2.

Analogically, the increase in the retarded Hamaker constant with Φ of the MoS_2 NPs, for the interacting systems "GO/MoS_2-$Pb_5(PO_4)_3Cl$," "PLA/MoS_2-$Pb_5(PO_4)_3Cl$," "GO/MoS_2-PbO_2," and "PLA/MoS_2-PbO_2" in the water medium (cf. Section 3.1), involves an enhancement of the corresponding vdW adsorption potentials.

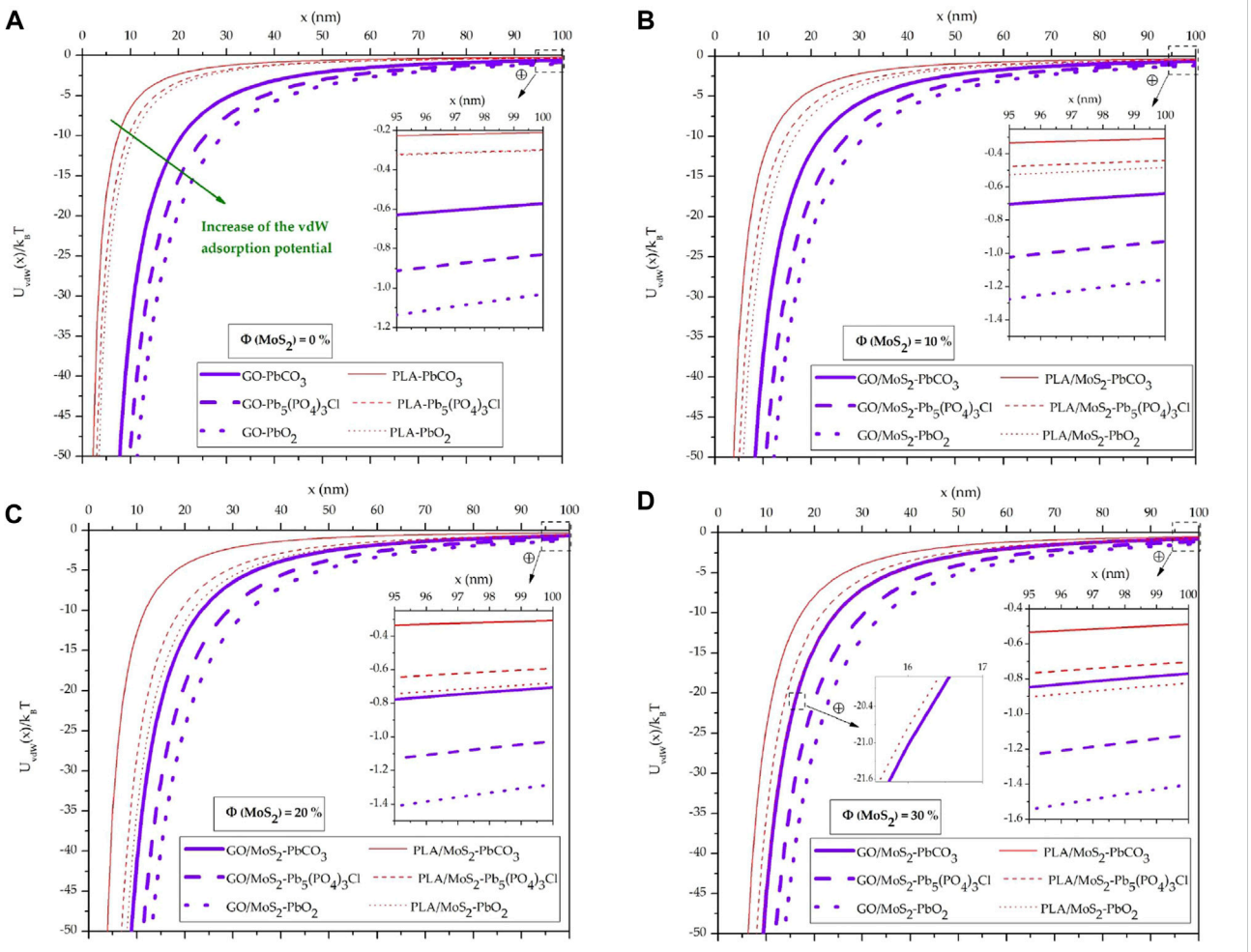

FIGURE 4
Evolution of the vdW adsorption potential between the GO/MoS_2 and PLA/MoS_2 nanocomposite adsorbents and the "$PbCO_3$, $Pb_5(PO_4)_3Cl$, and PbO_2" lead adsorbates in a water medium: **(A)** Φ = 0%, **(B)** Φ = 10%, **(C)** Φ = 20%, and **(D)** Φ = 30%.

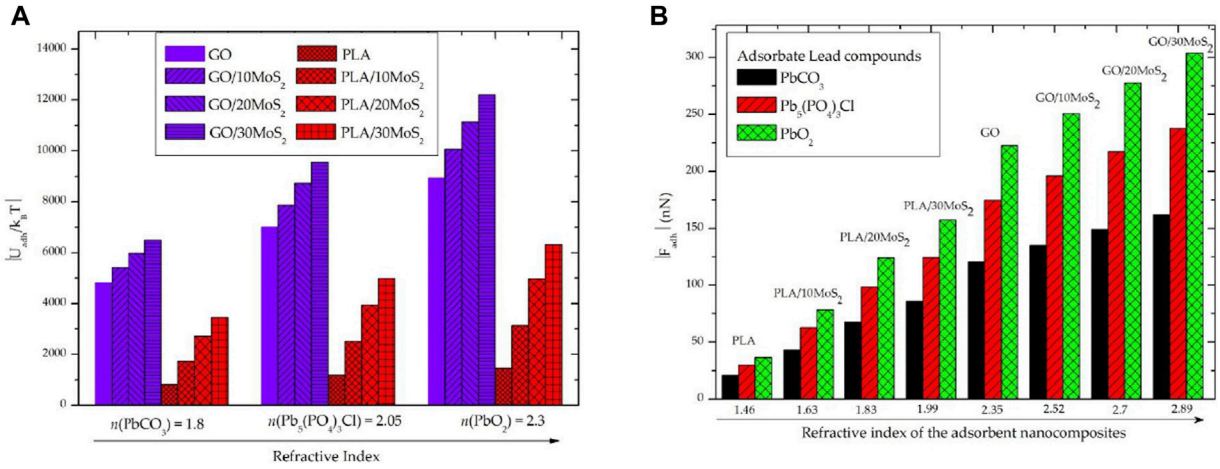

FIGURE 5
Evolution of the vdW adhesion energy and force corresponding to the physical adsorption of the "$PbCO_3$, $Pb_5(PO_4)_3Cl$, and PbO_2" lead compound adsorbates onto "GO/MoS_2 and PLA/MoS_2" nanocomposite adsorbents in a water medium as a function of the refractive index: **(A)** adhesion energy and **(B)** adhesion force.

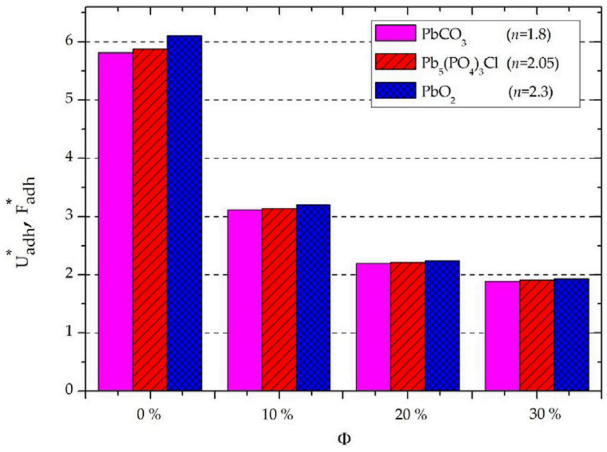

FIGURE 6
Scaled vdW energy and force using Eq. 8 with the same lead adsorbate radius Rp = cte.

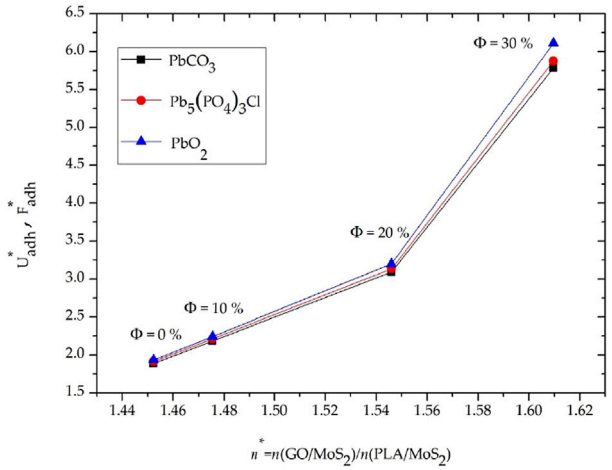

FIGURE 7
Evolution of the scaled energy and force as a function of the refractive index ratio n^* considering the lead compounds have the same radius R_p = Cte.

3.2.2 Effect of the lead compounds and nanocomposite types

3.2.2.1 Effect of nanocomposite adsorbent types

To examine the effect of the adsorbent type on the vdW adsorption potential, we have collected, in Figure 4, the evolution of $U_{vdW}(x)/k_BT$ of the adsorbents, "GO/MoS_2 and PLA/MoS_2," and the adsorbates, "$PbCO_3$, $Pb_5(PO_4)_3Cl$, and PbO_2," in the water medium separately for fixed Φ of MoS_2 NPs. For Φ = 0%, 10%, and 20% (Figures 4A–C), $U_{vdW}(x)/k_BT$ for the interacting media "GO/MoS_2-lead compounds" (bold violet curves) in the water medium is gradually more important than those for "PLA/MoS_2-lead compounds" (thin red curves) along the separation distance x.

Qualitatively, these findings indicate that the physical adsorption of the lead compounds is higher on the GO/MoS_2 nanocomposite surface than the PLA/MoS_2 one. However, for Φ = 30% and at $x > 28.4$ nm (Figure 4D), $U_{vdW}(x)/k_BT$ for the interaction between PLA/MoS_2-PbO_2 becomes more important than the interaction between GO/MoS_2-$PbCO_3$ in the water medium. This can be explained by the fact that, on the one hand, the dispersion interactions for both PLA/MoS_2-PbO_2 and GO/MoS_2-$PbCO_3$ in the water medium are reduced at large separation (retardation effect) and, consequently, the polar vdW interactions that no suffer retardation effects become the driving interactions. On the other hand, by referring to Eq. 4 and Tables 2, 3, the elevated dielectric constant of the $GO/30MoS_2$ and $PbCO_3$ of 33.58 and 18.6, respectively, compared with $PLA/30MoS_2$ and PbO_2 of 5.90 and 12.5, respectively, yields the non-retarded Hamaker constant's lower value for the interacting media GO/MoS_2-$PbCO_3$

($A_{v=0}$ = 0.76 10^{-21} J) compared to PLA/MoS_2 and PbO_2 ($A_{v=0}$ = 1.92 10^{-21} J) in the water medium.

Particularly, this result highlights that despite the poor contribution of the polar Keesom–Debye interactions to the total vdW interactions at close separation, it becomes the driving force for the physical adsorption at large separation.

Thereafter, we examine the strength of the adhesion energy and force that corresponds to the vdW adsorption. The adhesion energy and force of the lead compounds with GO/MoS_2 and PLA/MoS_2 nanocomposites surface were calculated using Eqs 2, 3. As shown in Figure 5, the vdW adhesion energy and force are, respectively, in the order of ×1,000.k_BT and ×100 nN. This is in good agreement with the order of magnitude of the non-covalent interactions scales of the microscopic systems [31] and then demonstrates the accuracy of our used analytics methods.

However, for each adsorbate type of lead compounds, U_{adh}/k_BT and F_{adh} were more important for GO/MoS_2 compared to those for PLA/MoS_2 nanocomposite adsorbent. Consequently, this demonstrates the increased physical adsorption stability of the lead compounds onto GO/MoS_2 compared to the PLA/MoS_2 adsorbent.

3.2.2.2 Effect of lead compound type

As shown in Figure 4, for the same nanocomposite adsorbent (GO/MoS_2 or PLA/MoS_2), we found that $U_{vdW}(x)/k_BT$ was more important in the order of the adsorbate type "PbO_2" > "$Pb_5(PO_4)_3Cl$" > "$PbCO_3$". Similarly, in Figure 5, this fact can be observed clearly in the vdW adhesion energy and force between lead compounds and the nanocomposite surface. As previously deduced from the Hamaker constant, this result demonstrates that the increase in the vdW adsorption is strongly associated with the increase in the London dispersion interactions that are proportional to an increase in the refractive index ("$n(PbO_2)$ = 2.3" > "$n(Pb_5(PO_4)_3Cl)$ = 2.05" > "$n(PbCO_3)$ = 1.8"). These basic findings are consistent with recent previous research conducted by Sato et al. [25] and Aoyama et al. [29], showing that the quantity of adsorbed particles increased with increasing the refractive indices of the particles.

So far, it has been shown that vdW adsorption in the water medium is enhanced by increasing London dispersion interactions for either the adsorbent or the adsorbate or both.

Eventually, it is important to find which interacting medium (adsorbent or adsorbate) has the greatest contribution to the physical vdW adsorption in the water medium. To this purpose, it is efficient to scale the vdW adhesion energy and force of the GO/MOS_2 to the PLA/MoS_2 nanocomposites for each given lead compound (at R_p = cte) and filling rate of the MoS_2 NPs as follows:

$$\mathbf{U^*_{adh}} = \mathbf{F^*_{adh}} = \frac{\mathbf{U_{adh}(GO/MoS_2)}}{\mathbf{U_{adh}(PLA/MoS_2)}}\Big|_{\mathbf{PbO_2, Pb_5(PO_4)_3Cl, PbCO_3, \Phi}} = \frac{\mathbf{A(GO/MoS_2)}}{\mathbf{A(PLA/MoS_2)}}\Big|_{\mathbf{PbO_2, Pb_5(PO_4)_3Cl, PbCO_3, \Phi}}. \quad (8)$$

As shown in Figure 6, there is little difference between U^*_{adh} for PbO_2, $Pb_5(PO_4)_3Cl$ and $PbCO_3$ adsorbate at fixed Φ. Consequently, this proves the poor contribution of the lead compound type on the adsorption energy and force.

Eventually, for all "PbO_2, $Pb_5(PO4)_3Cl$, and $PbCO_3$" adsorbates, U^*_{adh} were ~6, ~3.1, ~2.2, and ~1.9, respectively, for Φ = 0%, 10%, 20%, and 30%. On the one hand, this result demonstrates the weak contribution of the adsorbate type to the vdW adhesion energy and force governing the physical adsorption. On the other hand, this reveals the higher dependency of the vdW adsorption energy and force on the adsorbent type, which is always higher for GO/MOS_2 than for PLA/MOS_2 nanocomposite.

Effectively, the decrease in the U^*_{adh} ratio with increasing the filling ratios in Figure 6 is caused by the reduction in the gap between the refractive indexes of the GO/MoS_2 and PLA/MoS_2 nanocomposites during filling with MoS_2 NPs. In fact, the refractive index of the PLA/MoS_2 and GO/MoS_2 adsorbents increases during filling until it converges to the refractive index of the MoS_2 NPs.

Figure 7 compiles the evolution of $U^*_{adh}$for the "PbO_2, $Pb_5(PO_4)_3Cl$, and $PbCO_3$" adsorbate as function of the refractive index ratio $n^\star = n(GO/MoS_2)/n(PLA/MoS_2)$ for Φ = 0%, 10%, 20%, and 30%.

Overall, it is observed in Figure 7 that $U^*_{adh}$and $n^\star$ curves provide the same profile behavior when increasing the filling rates of MoS_2. This result demonstrates that the London dispersion interactions on the PLA/MoS_2 and GO/MoS_2 adsorbent surface were the driving interactions for increasing the vdW adsorption (i.e., the physical adsorption).

Future studies could investigate the vdW adsorption for higher filling rates (Φ > 30%), in which U^*_{adh} continues to decrease to reach 1 for purely MoS_2 adsorbent (Φ = 100%). In this insight, a forthcoming experimental study may investigate the adsorbent nanocomposite stability and efficiency under real conditions, in which the vdW adsorption may be improved by decreasing temperature and varying the morphological properties, such as porosity and roughness.

Furthermore, it is important to note that the adhesion energy and force (Figure 6) constitute the threshold adhesion for the desorption of the lead compounds that may occur under the action of the water flow during nanofiltration or purification processes. Consequently, future theoretical and experimental research should be devoted to valorizing the findings of this study to examine the effect of the water velocity on the desorption of insoluble lead compounds during the nano/microfiltration process.

4 Conclusion

In summary, the physical adsorption of the $PbCO_3$, PbO_2, and $Pb_5(PO_4)_3Cl$ compounds from water onto GO/MoS_2 and PLA/MoS_2 nanocomposite surface were theoretically investigated on the basis of the Lifshitz theory. The physical adsorption behavior was analyzed in terms of the Hamaker constant, vdW adsorption potential, vdW adhesion energy, and force.

From the analysis of the Hamaker constant at a large separating distance, it is shown that the vdW interactions, which are responsible for the physical adsorption of the insoluble compounds, are dominated over 90% by the London disperse interactions tuned by the refractive index of the adsorbent and adsorbate.

Collectively, for PLA and GO matrixes, it was demonstrated that the physical adsorption of the lead compounds from water was greater on the GO surface, which exhibits a higher refractive index. However, under the filling of the PLA and GO matrixes with MoS_2 nanoparticles, a significant enhancement of the Hamaker constant, vdW adsorption potential, vdW adhesion energy, and force was demonstrated.

Overall, the physical adsorption is essentially enhanced by increasing the refractive index of the PLA/MoS_2 and GO/MoS_2 adsorbents, which can be allowed using an MoS_2 nanoparticle.

These findings provide potential qualitative and quantitative recommendations for future experimental studies for the removal of lead compounds from water using GO/MoS_2 and PLA/MoS_2 nanocomposites.

Data availability statement

The original contributions presented in the study are included in the article/supplementary material. Further inquiries can be directed to the corresponding authors.

Author contributions

Conceptualization: NM, AA, and NA; methodology: NM and AA; software: NM; validation: NM and AA; formal analysis: NM, HO, and SH; investigation: NM and AA; resources: NM and NA; data curation: NM; writing—original draft preparation: NM, NA, and AA; writing—review and editing: NM, SH, AA, and HO; visualization: NM; supervision: NM, NA, SH, and AA; project administration: NM, NA, and AA; funding acquisition: NA and AA. All authors have read and agreed to the published version of the manuscript.

Funding

This research was funded by the Deanship of Scientific Research at King Khalid University under Grant no. RGP.2/182/43. Additionally, this research was funded by Princess Nourah Bint Abdulrahman University Researchers Supporting Project number (PNURSP2023R19), Princess Nourah Bint Abdulrahman University, Riyadh, Saudi Arabia.

Acknowledgments

The authors extend their appreciation to the Deanship of Scientific Research at King Khalid University for funding this work through Large Groups Project under Grant no. RGP.2/182/43. Also, the authors express their gratitude to Princess Nourah bint Abdulrahman University Researchers Supporting Project number (PNURSP2023R19), Princess Nourah bint Abdulrahman University, Riyadh, Saudi Arabia.

Conflict of interest

The authors declare that the research was conducted in the absence of any commercial or financial relationships that could be construed as a potential conflict of interest.

Publisher's note

All claims expressed in this article are solely those of the authors and do not necessarily represent those of their affiliated organizations or those of the publisher, the editors, and the reviewers. Any product that may be evaluated in this article, or claim that may be made by its manufacturer, is not guaranteed or endorsed by the publisher.

References

1. Darren L, Michael S, Casey F, Christina B-S, Stephen H, Mallikarjuna N, et al. Lead particle size fractionation and identification in newark, newersey's drinking water. *Environ Sci Tech* (2020) 54(21):13672–9. doi:10.1021/acs.est.0c03797

2. Shu C, Lu C, King C, Joseph L, John F, Kelvin K. Unraveling the causes of excess lead in drinking water supply systems of densely populated high-rise buildings in Hong Kong. *Environ Sci Tech* (2020) 54(22). doi:10.1021/acs.est.0c03232

3. Yan Z, Yuanyuan Z, Yi-Pin L. Fast detection of lead Dioxide (PbO2) in chlorinated drinking water by a two-stage iodometric method. *Environ Sci Tech* (2010) 2 44(4): 1347–52. doi:10.1021/es902299b

4. Yu-Cheng P, Yi-Fang L, Yi-Pin L. Release of particulate lead from four lead corrosion products in drinking water: A laboratory study coupled with microscopic observations and computational fluid dynamics. *Environ Sci Tech* (2022) 56(17): 12218–27. doi:10.1021/acs.est.2c02461

5. Jing L, Jian-su M. Risk assessment of lead emissions from anthropogenic cycle. *Trans Nonferrous Met Soc China* (2016) 26:248–55. doi:10.1016/S1003-6326(16)64148-1

6. Lu C, Joseph L, Fung Y. Prediction of lead leaching from galvanic corrosion of lead containing components in copper pipe drinking water supply systems. *J Hazard Mater* (2022) 436:129169. doi:10.1016/j.jhazmat.2022.129169

7. World Human Organization. Lead in drinking-water: Health risks, monitoring and corrective actions. WHO TEAM Environment, *Clim Change Health Water Sanitation, Hyg Health* (2022) 1–26. Available at: https://www.who.int/publications/i/item/9789240020863 [Accessed January 15, 2023]

8. Alberto F, Mir D, Ali G. *4 - application of nanotechnology in drinking water purification" in Water Purification*. Cambridge, USA: Elsevier Academic Press (2017). 119–67. doi:10.1016/B978-0-12-804300-4.00004-6

9. Satinder A. Chapter 1 - overview of advances in water purification techniques. In: *Advances in water purification techniques*. Calabash, NC, United States: Elsevier (2019). 1–15. doi:10.1016/B978-0-12-814790-0.00001-6

10. Antonio G, Luis G, Miguel V. Applications of advanced oxidation processes (AOPs) in drinking water treatment. In: *The handbook of environmental chemistry*. Cham, Switzerland: Springer Nature (2019). 66–149. doi:10.1007/978-3-319-76882-3

11. Iervolino G, Zammit I, Vaiano V, Luigi R. Limitations and prospects for wastewater treatment by UV and visible-light-active heterogeneous photocatalysis: A critical review. *Top Curr Chem* (2020) 378:7. doi:10.1007/s41061-019-0272-1

12. Muhammad H, Farwa N, Muhammad Z, Farkhanda K, Asma H, Muhammad A. Chapter 23 - applications of coagulation-flocculation and nanotechnology in water treatment. In: *Micro and nano technologies, aquananotechnology*. Elsevier (2021). 533–58. doi:10.1016/B978-0-12-821141-0.00012-4

13. Yang Z, Zhou Y, Feng Z, Rui X, Zhang T, Zhang Z. A review on reverse osmosis and nanofiltration membranes for water purification. *Polymers* (2019) 11:1252. doi:10.3390/polym11081252

14. Lide DR. *CRC handbook of chemistry and physics*. 88Th ed. Boca Raton, FL: CRC Press, Taylor & Francis (2007). 4–64/65.

15. Gu T, Qin S, Wu X. Thermal behavior of pyromorphite (Pb10(PO4)6Cl2): *In situ* high temperature powder X-ray diffraction study. *Crystals* (2020) 10:1070. doi:10.3390/cryst10121070

16. Pouran P, Ali T, Mohsen T, Mehrorang G, Sepahdar H. Chapter 1 - fundamentals of adsorption technology" in interface science and technology. *Elsevier* (2021) 33:1–70. doi:10.1016/B978-0-12-818805-7.00001-1

17. Tawfik S. Chapter 2 - adsorption technology and surface science" in interface science and technology. *Elsevier* (2022) 34:39–64. doi:10.1016/B978-0-12-849876-7.00006-3

18. James C. Chapter 1 - an overview and some uninteresting history of physisorption. In: *Surface area and porosity determinations by physisorption*. 2nd ed. Elsevier (2020). 1–57. doi:10.1016/B978-0-12-818785-2.00001-5

19. Arunima N, Brij B, Nupur K, Shreya K. *Chapter 5 - graphene oxides and its composites as new generation adsorbents for remediation of toxic pollutants from water: An overview" in Sustainable Materials for Sensing and Remediation of Noxious Pollutants*. Elsevier (2022). 65–85. doi:10.1016/B978-0-323-99425-5.00014-1

20. Souravi B, Shubham R, Mousumi M, Sukhen D. 22 - metal oxide/graphene nanocomposites and their biomedical applications. In: *Metal oxides, metal oxides for biomedical and biosensor applications*. Elsevier (2022). 569–84. doi:10.1016/B978-0-12-823033-6.00020-X

21. Luc A. 9—Synthesis, properties, environmental and biomedical applications of polylactic acid. In: *Plastics design library, handbook of biopolymers and biodegradable plastics*. New York: William Andrew Publishing (2013). 171–88. doi:10.1016/B978-1-4557-2834-3.00009-4

22. Ashutosh P, Ranjna S, Sudha U, Mitali M, Virendra K, Lalit S, et al. Chapter 12 - production and applications of polylactic acid" in biomass, biofuels. *Biochemicals, Elsevier* (2021) 309–57. doi:10.1016/B978-0-12-821888-4.00013-7

23. Levna C, Aswini P, Kumar. V, Aneesh P. Chapter 19 - MoS2, a new perspective beyond graphene. In: *Micro and nano technologies, fundamentals and properties of multifunctional nanomaterials*. Elsevier (2021). 499–541. doi:10.1016/B978-0-12-822352-9.00018-3

24. Chang L, Qingmiao W, Feifei J, Shaoxian S. Adsorption of heavy metals on molybdenum disulfide in water: A critical review. *J Mol Liquids* (2019) 292:111390. doi:10.1016/j.molliq.2019.111390

25. Sato N, Aoyama Y, Yamanaka J, Toyotama A, Okuzono T. Particle adsorption on hydrogel surfaces in aqueous media due to van der Waals attraction. *Sci Rep* (2017) 7:6099. doi:10.1038/s41598-017-06257-1

26. Antonius A, Meret A, Ronald J, Dominik R, Thérèse S, Tamar K, et al. Viruses at solid–water interfaces: A systematic assessment of interactions driving adsorption. *A Syst Assess Interactions Driving Adsorption Environ Sci Tech* (2016) 50:732–43. doi:10.1021/acs.est.5b04644

27. Emily M, Kenneth R, Jacob I. Recent progress in understanding hydrophobic interactions. *PNAS* (2006) 103:15739–46. doi:10.1073/pnas.0606422103

28. Christian W, Maria S. Effect of surface hydrophobicity on adsorption and relaxation kinetics of albumin and fibrinogen: Single-species and competitive behavior. *Langmuir* (2001) 17(10):3006–16. doi:10.1021/la0017781

29. Yurina A, Naoko S, Akiko T, Tohru O, Junpei Y. Particle adsorption on polymer gel surface driven by van der Waals attraction. *Chem Soc Jpn* (2022) 95. 2. doi:10.1246/bcsj.20210356

30. Mahdhi N, Alsaiari NS, Alzahrani M, Katubi M, Amari A, Hammami S. Theoretical investigation of the adsorption of cadmium iodide from water using polyaniline polymer filled with TiO2 and ZnO nanoparticles. *Water MDPI* (2021) 13:2591. doi:10.3390/w13182591

31. Israelachvili J. *Intermolecular and surface forces*. 3rd ed. Burlington, NJ, USA: Academic Press (2011). p. 107–316.

32. Keesom H. The cohesion forces in the theory of Van der Waals. *Proc Ser B Phys Sci* (1921) 23:943–8. Available at: https://ui.adsabs.harvard.edu/abs/1921KNAB.23.943K (Accessed January 15, 2023).

33. Rimai D, Quesnel D. Chapter 3 - particle adhesion. In: *Adhesion science and engineering*. Elsevier Science B.V (2002). p. 139–91. doi:10.1016/B978-044451140-9/50003-2

34. Russel W, Saville D, Schowalter W. Dispersion forces. In: *Colloidal dispersions, cambridge monographs on mechanics*. Cambridge: Cambridge University Press (1989). p. 129–61. doi:10.1017/CBO9780511608810.0081

35. London F. The general theory of molecular forces. *Trans Faraday Soc* (1937) 33:8–26. doi:10.1039/TF937330008B

36. John G. Approximate expressions for retarded van der waals interaction. *J Colloid Interf Sci* (1981) 83(1):138–45. doi:10.1016/0021-9797(81)90018-7

37. Nicolás R, Francisco C, Valeria T, Claudio J, Ricardo F, Leonardo B. Complex dielectric permittivity of engineering and 3D-printing polymers at Q-band. *J Infrared Milli Terahz Waves* (2018) 39:1140–7. doi:10.1007/s10762-018-0528-9

38. Si-Ting S, Hang W, Dong H, Ying-Li D, Yang Z, Dong-Po S, et al. Refractive index engineering as a novel strategy toward highly transparent and tough sustainable polymer blends. *Chin J Polym Sci* (2020) 38:1335–44. doi:10.1007/s10118-020-2439-1

39. Prokhorov E, Barquera-Bibiano Z, Manzano-Ramírez A, Luna-Barcenas G, Kovalenko Y, Hernández-Landaverde A, et al. New insights in graphene oxide dielectric constant. *Mater Res Express* (2019) 6:085622. doi:10.1088/2053-1591/ab22f0

40. Politano G, Versace C, Vena C, Castriota M, Ciuchi F, Fasanella A, et al. Physical investigation of electrophoretically deposited graphene oxide and reduced graphene oxide thin films. *J Appl Phys* (2016) 120:195307. doi:10.1063/1.4968000

41. Beal R, Hughes H. Kramers-Kronig analysis of the reflectivity spectra of 2H-MoS2, 2H-MoSe2 and 2H-MoTe2. *J Phys C: Solid State Phys* (1979) 12:881–90. doi:10.1088/0022-3719/12/5/017

42. Hui Z, Yaoguang M, Yi W, Xin R, Ziang X, Wei W, et al. Measuring the refractive index of highly crystalline monolayer MoS2 with high confidence. *Sci Rep* (2015) 5:8440. doi:10.1038/srep08440

43. Young K, Frederikse H. Compilation of the static dielectric constant of inorganic solids. *J Phys Chem Reference Data* (1973) 2:313–410. doi:10.1063/1.3253121

44. Joseph R, Dudley S. "The dielectric constant of mineral powders: Rensselaer polytechnic institute engineering and science series, No. 52," in *The American Mineralogist*. Montana, United States: Literary Licensing, LLC (2013) 21 (2), 118.

45. Raza A, Faizan M, Sultana I, Ghulam M, Shahid A, Aneeqa B, et al. Morphology and dielectric studies of natural fibers and PbO2 based flexible composite sheets for potential energy storage applications. *J Electron Mater* (2020) 49:1896–903. doi:10.1007/s11664-019-07877-1

46. Weast RC. *Handbook of chemistry and physics*. 68th ed. Boca Raton, Florida: CRC Press Inc. (1987). B-100.

47. Fernández P, Mulev Y, Goodwin H, Sengers L. A database for the static dielectric constant of water and steam. *J Phys Chem Ref Data* (1995) 24:33–70. doi:10.1063/1.555977

48. Karkkainen K, Sihvola A, Nikoskinen K. Effective permittivity of mixtures: Numerical validation by the FDTD method. *IEEE Trans Geosci Remote Sensing* (2000) 38:1303–8. doi:10.1109/36.843023

49. Vadim M. Introduction to the Maxwell garnett approximation: Tutorial, *J Opt Soc Am* (2016) 33. 1244, doi:10.1364/JOSAA.33.001244